2019 IEEE/RSJ International Conference on Intelligent Robots and Systems (IROS)
Macau, China, November 4-8, 2019

Robust Trajectory Planning for a Multirotor against Disturbance based on Hamilton-Jacobi Reachability Analysis

Hoseong Seo, Donggun Lee, Clark Youngdong Son, Claire J. Tomlin, and H. Jin Kim

Abstract— **Ensuring safety in trajectory planning of multirotor systems is an essential element for risk-free operation. Even if the generated trajectory is known to be safe in the planning phase, unknown disturbance during an actual operation can lead to a dangerous situation. This paper proposes safety-guaranteed receding horizon planning against unknown, but bounded, disturbances. We first characterize forward reachable set (FRS) of the system, the set of states after a certain duration considering all possible disturbances, using Hamilton-Jacobi (HJ) reachability analysis. To compute the FRSs in real-time, we conservatively approximate the true FRS and perform ellipsoidal parameterization on the FRSs. Using the FRSs, we can plan a robust trajectory that avoids risky regions and rapidly re-plan the trajectory when the system encounters sudden disturbance. The proposed method is validated through an experiment of avoiding obstacles in a wind.**

I. Introduction

Safety guarantee is an important topic in fully utilizing high maneuverability of multirotor systems for a broad range of applications. Such importance has led to recent works on generating safe flight trajectories for multirotor systems in cluttered environments. The authors of [1] proposed a method for planning a time-parameterized trajectory in a confined space. With the aid of a sampling-based planner, collision-free waypoints were specified and used to enforce the planned trajectory to pass through those waypoints. Similar approaches were proposed in [2], [3] with consideration of a collision cost in optimizing the flight path. Some works tried to decompose a cluttered space into free space and occupied space. The free space was modeled as rectangular grids [4] or maximal ellipsoids [5] and then considered as inequality constraints in trajectory optimization.

Although many existing works on trajectory planning offer appealing solutions for safe flight, the generated trajectory may not be sufficient to guarantee safety if affected by unknown disturbances in actual environments. Various sources such as ground effect, sudden gust, modeling errors, and the rotor drags can act as disturbance for multirotors [6]. Because they are not only difficult to model but also unknown a priori, trajectory tracking error must occur even though a controller tries to reject disturbance as much as possible.

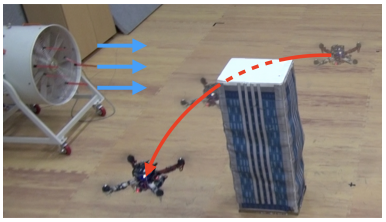

Fig. 1. A multirotor avoids an obstacle in an environment with gust.

Our objective is to plan a safety-guaranteed flight trajectory for multirotor systems considering tracking error due to unknown disturbance. To obtain robustness, we have to figure out how far the error can be propagated due to disturbance, namely forward reachable set (FRS) of the error dynamics. We utilize the Hamilton-Jacobi (HJ) reachability analysis [7] as a tool for computing the FRSs with the assumption that disturbances are bounded. By considering the expected region of the error, the generated trajectory is guaranteed to be safe because the error does not exceed the FRSs whenever the disturbance bounds are satisfied.

We also concentrate on a fast computation of a robust flight trajectory. When the system suddenly runs into different disturbance, the previously computed trajectory no longer ensures safety since the current disturbances may exceed the pre-set bounds. In this case, the FRSs must be re-evaluated according to the increased disturbance bounds, and the flight trajectory must be rapidly re-planned to maintain the robustness of the entire flight. We introduce an ellipsoidal parameterization on the FRSs based on the solution of the HJ reachability analysis. With this approximation, we propose a propagation law for the FRSs, which enables us to compute the robust flight trajectory in real-time.

A. Related Works

In [8], the safety funnel libraries were proposed for a finite number of motion primitives based on the Lyapunov analysis. As a kind of the FRSs, those safety funnels were computed for each primitive via the sum of squares programming in the offline phase and then combined during the online phase for avoiding obstacles. A heavy computation load was required for the offline phase, and reference trajectories must be precomputed before constructing the funnel libraries. In [9], FRSs for the closed-loop dynamics of the multirotor were generated similarly to [8]. By estimating the rotor drag rather

This material is based upon work supported by the Ministry of Trade, Industry & Energy(MOTIE, Korea) under Industrial Technology Innovation Program (No. 10051673).

Hoseong Seo is with the Automation and Systems Research Institute and Department of Mechanical and Aerospace Engineering, Seoul National University, Seoul, South Korea. hosung37@snu.ac.kr

Donggun Lee is with the Department of Mechanical Engineering, University of California, Berkeley, USA. donggun_lee@berkeley.edu

Clark Youngdong Son is with the Department of Mechanical and Aerospace Engineering, Seoul National University, Seoul, South Korea. clark.y.d.son@snu.ac.kr

Claire J. Tomlin is with the Department of Electrical Engineering and Computer Sciences, University of California, Berkeley, USA. tomlin@eecs.berkeley.edu

H. Jin Kim is with the Institute of Engineering Research and Department of Mechanical and Aerospace Engineering, Seoul National University, Seoul, South Korea. hjinkim@snu.ac.kr

than considering it as unknown disturbance, less conservative FRSs were computed. However, FRSs must be re-computed if some parameters of the controller change.

In [10], [11], a trajectory planning problem was formulated as a pursuit-evasion game between a planning system and a tracking system. The HJ reachability analysis was conducted on the relative dynamics (i.e. the difference between the planning and tracking models) to compute the maximum tracking error in the offline phase. For computational simplicity, [10] used the planning model of constant speed which resulted in overly conservative error bounds for the relative dynamics. Multiple planning models with various speeds were employed and then an appropriate planning model was selected depending on the complexity of the surroundings in [11]. But the speed of planning systems must be determined before the reachability analysis and the computed error bounds were valid only for predefined planning systems.

In [12], [13], robust forward invariant tubes and a robust model predictive control (MPC) algorithm were proposed based on differential inequalities. The invariant tubes also presented theoretical enclosures of the system under disturbances. The tube-MPC could be solved online, but complex computation was required to generate the tubes since a matrix-valued optimal control problem must be solved.

B. Contributions

- Characterization of the expected region for tracking error of the multirotor based on HJ reachability analysis – We investigate an analytic solution of the reachable set of the multirotor under the bounded disturbance, which is not mainly addressed in the existing works on real-time trajectory planning.
- A real-time propagation law for the error FRSs which guarantees the safety of the planned trajectory
  – Most existing works require reformulation or re-computation of the reachable set from scratch when parameters such as control gains and disturbance bounds are changed; however, our work presents a closed-form solution of the reachable set as ellipsoids.

C. Outline

We formulate a problem and define the error FRS in Section II. Section III describes the analytic solution of the HJ reachability analysis and characterizes FRSs of tracking errors. A conservative, but computationally efficient, approximation on the FRSs and the FRS-based robust planning algorithm are described in Section IV. Experimental validation and conclusion are followed in Sections V and VI.

II. Problem Formulation

We consider the following simplified 8-state multirotor dynamics with external disturbance in the acceleration channel:

$$\begin{aligned} \ddot{r} &= \frac{F}{m}\begin{bmatrix}\cos\phi\sin\theta\\ -\sin\phi\\ \cos\phi\cos\theta\end{bmatrix} + \begin{bmatrix}0\\0\\-G\end{bmatrix} + w,\\ \dot{\phi} &= \dot{\phi}_d,\\ \dot{\theta} &= \dot{\theta}_d, \end{aligned} \tag{1}$$

where $r \in \mathbb{R}^3$ is the position of the multirotor, $m \in \mathbb{R}$ is the mass of the multirotor, $F \in \mathbb{R}$ is the total thrust exerted by the multirotor, ϕ and $\theta \in \mathbb{R}$ are the roll and pitch angles of the multirotor, $G \in \mathbb{R}$ is the gravitational acceleration, $\dot{\phi}_d$ and $\dot{\theta}_d$ are the desired roll and pitch rates, and $w \in \mathbb{R}^{n_w}$ is the mass-normalized external disturbance with $n_w = 3$. It is assumed that the heading angle of the multirotor can always be maintained as zero, and roll/pitch rates track the desired command sufficiently well. The state and input are defined as $x = [r^\top \dot{r}^\top \phi\ \theta]^\top \in \mathbb{R}^{n_x}$, and $u = [F\ \dot{\phi}_d\ \dot{\theta}_d]^\top \in \mathbb{R}^{n_u}$ with $n_x = 8$ and $n_u = 3$. The dynamics can be written as $\dot{x} = f(x(t), u(t), w(t))$.

The FRS $\mathscr{X}(t) \subset \mathbb{R}^{n_x}$ is the set of all states to which a system can be derived from the given initial set of states $\mathscr{X}_0 \subset \mathbb{R}^{n_x}$ after a certain duration $t > 0$, considering all possible inputs and disturbances [14]. For general nonlinear systems, exact computation of the FRSs, as well as its propagation law, is intractable. We linearize the system around nominal states and inputs, which are assumed to be known, to reduce the complexity in computing the FRSs. For multirotor systems, the assumption on known nominal values is not restrictive because we can take advantage of a structural property such as the differential flatness [15], [16].

Let us denote the nominal states and inputs as $\underline{x}(t) \in \mathbb{R}^{n_x}$ and $\underline{u}(t) \in \mathbb{R}^{n_u}$. The dynamics of the error state $e(t) := x(t) - \underline{x}(t)$ with linearization around $\underline{x}(t)$ and $\underline{u}(t)$ can be expressed as follows.

$$\begin{aligned} \dot{e}(t) = A(t)e(t) + B(t)(u(t) - \underline{u}(t)) + D(t)w(t)\\ + \xi(e(t), u(t) - \underline{u}(t), w(t)), \end{aligned} \tag{2}$$

where $A(t) := \partial f/\partial x|_{(\bar{x},\bar{u},0)} \in \mathbb{R}^{n_x \times n_x}$, $B(t) := \partial f/\partial u|_{(\bar{x},\bar{u},0)} \in \mathbb{R}^{n_x \times n_u}$, $D(t) := \partial f/\partial w|_{(\bar{x},\bar{u},0)} \in \mathbb{R}^{n_x \times n_w}$ are linearized system matrices at the nominal states and inputs. To simplify our analysis, we make the following assumptions.

Assumption 1. The linearization error $\xi \in \mathbb{R}^{n_x}$ is negligible near $\underline{x}(t)$.

Assumption 2. The control policy is composed of an affine feedback and a feedforward term as

$$u(t) = K(t)e(t) + \underline{u}(t), \tag{3}$$

where $K(t) \in \mathbb{R}^{n_u \times n_x}$, and the feedback gains are known a prior to compute the FRSs.

Note that Assumption 1 can be removed if some conservative approximations on ξ such as nonlinearity bounders [13] are explicitly considered in the error dynamics, but it is out of the scope of this work.

The resultant error dynamics can be expressed as

$$\dot{e}(t) = \Phi(t)e(t) + D(t)w(t), \tag{4}$$

where $\Phi(t) = A(t) + B(t)K(t)$. We now define the FRS $\mathscr{E}(t) \subset \mathbb{R}^{n_x}$ of the error system (4) as

$$\mathscr{E}(t) = \left\{ y \,\middle|\, \begin{array}{l} \forall \tau \in [0,t],\ \forall w(\tau) \in \mathbb{W},\\ \dot{e}(\tau) = \Phi(\tau)e(\tau) + D(\tau)w(\tau),\\ e(0) \in \mathscr{E}_0,\ y = e(t) \end{array} \right\}, \tag{5}$$

where $\mathscr{E}_0$ is the initial set of error states, and $\mathbb{W} \subset \mathbb{R}^{n_w}$ is

an admissible set for disturbances. Note that the FRS of the original system (1) is the translation of the error state FRS with $\underline{x}(t)$, namely $\mathscr{X}(t) = \mathscr{E}(t) + \underline{x}(t)$.

In order to plan the safety-guaranteed flight trajectory of the multirotor, we formulate the following optimization problem that can be solved in a receding horizon manner:

$$\begin{aligned} \min_{\underline{u}(t)} \quad & l_f(\underline{x}(T)) + \int_0^T l(\underline{x}(t), \underline{u}(t))\, dt \\ \text{s.t} \quad & \dot{\underline{x}}(t) = f(\underline{x}(t), \underline{u}(t), 0), \\ & \underline{x}(0) = x_0, \\ & c(\mathscr{X}(t)) > 0, \\ & \mathscr{X}(t) = \mathscr{E}(t) + \underline{x}(t) \\ \text{with} \quad & \dot{\mathscr{E}}(t) = g(\mathscr{E}(t)), \\ & \mathscr{E}(0) = \mathscr{E}_0, \end{aligned} \tag{6}$$

where x_0 is the initial state, l is the stage cost, l_f is the terminal cost, c represents the nonlinear constraints such as collision avoidance, g represents the propagation of the FRS $\mathscr{E}(t)$, and $T > 0$ is the prediction horizon. Note that the constraints c in (6) ensure that the system avoids risky regions whenever disturbances are bounded in $\mathbb{W}$.

From Assumption 2, we can divide the robust trajectory planning problem into two steps: the computation of $\mathscr{E}(t)$ and the optimization on $\underline{x}(t), \underline{u}(t)$ considering $\mathscr{E}(t)$. Given the initial guess on $\underline{x}(t)$ and $\underline{u}(t)$, $\mathscr{E}(t)$ is computed and then used to find the optimal $\underline{x}(t)$ and $\underline{u}(t)$ which robustly satisfy the constraints. The next section presents how to find analytic expressions of $\mathscr{E}(t)$ based on the reachability analysis.

III. Hamilton-Jacobi Reachability Analysis

This section aims to find the maximal reachable set of the error state considering adversary disturbances. To compute the error state FRS $\mathscr{E}(t)$, we consider an optimization problem of the reachability with the level set approach [14].

A. The reachability problem

We first define a convex function h, which satisfies $\mathscr{E}_0 = \{y | h(y) \leq 0\}$. The function h encodes information to determine whether an initial error is inside or outside $\mathscr{E}_0$. Consider a cost functional J defined as

$$J(e, w, t) = h(e(t)) + \int_0^t L(w(\tau))\, d\tau, \tag{7}$$

where the function L is the running cost detailed later. The value function V is defined as the minimum of J among all possible disturbances, namely

$$V(e, t) = \min_w J(e, w, t). \tag{8}$$

Since the worst case disturbance is expected to increase tracking errors, the disturbance tries to minimize J so that the zero level set of the value V can be expanded as much as possible.

The Hamilton-Jacobi equation of (8) can be derived from the dynamic programming principle [17]. The initial value HJ PDE is determined as

$$\begin{aligned} & \frac{\partial V}{\partial t} + \max_w \left(\frac{\partial V}{\partial e} \cdot \dot{e}(t) - L(w(t)) \right) = 0 \\ & V(e, 0) = h(e(0)). \end{aligned} \tag{9}$$

To consider the admissible set of disturbance, we use the following function as the running cost L,

$$L(w(t)) = \begin{cases} 0 & w(t) \in \mathbb{W} \\ \infty & w(t) \notin \mathbb{W}. \end{cases} \tag{10}$$

The Hamiltonian H is defined as the maximum value of the inner product of the error dynamics and the value gradient $\lambda := \partial V / \partial e \in \mathbb{R}^{n_x}$,

$$H(\lambda, t) = \max_{w \in \mathbb{W}} \lambda \cdot \big(\Phi(t) e(t) + D(t) w \big). \tag{11}$$

The optimal disturbance $w^\star(t)$ can steer an error state in the zero level set of $V(e,0)$ to the zero level set of $V(e,t)$. Consequently, the error state FRS after time t can be represented as

$$\mathscr{E}(t) = \{ e | V(e, t) \leq 0 \}. \tag{12}$$

B. Computation of the value function

The HJ reachability analysis provides the quantitative expression of the FRS. But it requires the solution of the initial value PDE, which is generally not tractable for high-dimensional systems. This section aims to find a tractable solution of the HJ PDE with the following assumption.

Assumption 3. The time-varying system matrix $\Phi(t)$ can be treated as a constant for a sufficiently small duration $[0, t]$. For convenience, we drop the time argument and use Φ as the constant system matrix during $\tau \in [0, t]$.

We now consider the following coordinate transform as proposed in [18], [19]

$$\eta(t) = \exp(-\Phi t) e(t), \tag{13}$$

and the dynamics of the transformed state is

$$\dot{\eta}(t) = \exp(-\Phi t) D(t) w(t). \tag{14}$$

For the system in the above form, the generalized Hopf formula [19] provides the solution for the value function as

$$V_\eta(\eta, t) = -\min_\lambda \left(h_\eta^*(\lambda(0)) + \int_0^t H_\eta(\lambda, \tau) d\tau - \eta \cdot \lambda \right), \tag{15}$$

where the superscript $*$ represents a convex conjugate of a function, and the subscript η represents the corresponding expression in the transformed coordinate, for instance $h(e(t)) = h(\exp(\Phi t)\eta(t)) = h_\eta(\eta(t))$. The Hamiltonian in (15) is

$$H_\eta(\lambda, t) = \max_{w \in \mathbb{W}} \lambda \cdot \big(\exp(-\Phi t) D(t) w \big). \tag{16}$$

Note that the Hamiltonian in η-coordinate does not contain state variables, unlike the original Hamiltonian.

Let us consider the following quadratic initial cost defined in the error space

$$h(e(0)) = e^\top Q_0^{-1} e - 1, \tag{17}$$

where $Q_0 \in \mathbb{S}^{n_x}_{++}$. Consequently, the initial set of error states can be expressed as the following ellipsoid,

$$\mathscr{E}_0 = \left\{ Q_0^{\frac{1}{2}} v \middle| ||v||_2^2 \leq 1 \right\}, \quad v \in \mathbb{R}^{n_x}. \tag{18}$$

Note that the initial sets of the error states and the transformed states are identical since $\eta(0) = e(0)$. Using the definition of the Fenchel-Legendre transform, the convex conjugate of $h_\eta(\eta(t))$, can be computed as

$$h_\eta^*(\lambda(t)) = \frac{1}{4}\lambda^\top \exp(-\Phi t) Q_0 \exp(-\Phi^\top t)\lambda + 1. \tag{19}$$

Before computing the Hamiltonian, we make the following assumption on the set of disturbances.

Assumption 4. Each channel of the disturbance is bounded, i.e. $|w_i(\tau)| \leq \bar{w}_i \in \mathbb{R}$, $\forall \tau \in [0,t]$ where the subscript i represents the i-th element of a vector with $i = 1, \ldots, n_w$.

The optimization in (16) results the following Hamiltonian

$$H_\eta(\lambda, t) = \sum_{i=1}^{n_w} |\lambda^\top \bar{D}_i(t)| \tag{20}$$

with the optimal disturbance

$$w_i^\star(t) = \text{sign}\left(\lambda^\top \bar{D}_i(t)\right) \bar{w}_i, \tag{21}$$

where $\bar{D}_i(t) := \exp(-\Phi t) D_i(t) \bar{w}_i \in \mathbb{R}^{n_x}$, and $D_i(t)$ is the i-th column of $D(t)$. Substituting (19) and (20) into (15) yields the value function expressed in η space and its convex conjugate as

$$\begin{aligned} V_\eta(\eta, t) &= -\min_\lambda \left(V_\eta^*(\lambda, t) - \eta \cdot \lambda\right), \\ V_\eta^*(\lambda, t) &= \frac{1}{4}\lambda^\top Q_0 \lambda + \sum_{i=1}^{n_w} \int_0^t |\lambda^\top \bar{D}_i(\tau)| d\tau + 1. \end{aligned} \tag{22}$$

C. Characterization of the FRS

The following proposition presents an explicit expression for the FRS based on the value function described in (22).

Proposition 1. Consider the dynamic system (14) with the initial set of states (18). Let $\mathscr{E}_\eta(t)$ be a set-valued function. If the value function satisfies (22), then

$$\mathscr{E}_\eta(t) = \left\{ Q_0^{\frac{1}{2}} v + \sum_{i=1}^{n_w} \int_0^t \bar{D}_i(\tau) \text{sgn}\left(v^\top Q_0^{-\frac{1}{2}} \bar{D}_i(\tau)\right) d\tau \right\}$$

is the FRS of system (14) after time t and $||v||_2^2 \leq 1$.

Proof. We use the property of Fenchel-Legendre transform [20] that the derivative of a convex function is the optimal argument of its conjugate. Let $\lambda^\star \in \mathbb{R}^{n_x}$ be the minimum argument of (22) as

$$V_\eta(\eta, t) = \eta^\top \lambda^\star - V_\eta^*(\lambda^\star, t). \tag{23}$$

Since $\lambda^\star$ is the minimizer and $V_\eta^*(\lambda, t)$ is convex on λ, we evaluate the first-order optimality condition and obtain

$$\begin{aligned} 0 &= \frac{\partial}{\partial \lambda}\left(\eta^\top \lambda - V_\eta^*(\lambda, t)\right)\Big|_{\lambda = \lambda^\star} \\ \Rightarrow \eta &= \frac{1}{2} Q_0 \lambda^\star + \sum_{i=1}^{n_w} \int_0^t \bar{D}_i(\tau) \text{sign}\left(\lambda^{\star\top} \bar{D}_i(\tau)\right) d\tau. \end{aligned} \tag{24}$$

Substituting (24) into (23) yields the other expression for the value function as

$$V_\eta(\lambda^\star, t) = \frac{1}{4}\lambda^{\star\top} Q_0 \lambda^\star - 1. \tag{25}$$

It is apparent that

$$V_\eta(\lambda^\star, t) \leq 0 \iff \lambda^\star \in \left\{ 2 Q_0^{-\frac{1}{2}} v \middle| ||v||_2^2 \leq 1 \right\}, \tag{26}$$

where $v := (1/2) Q_0^{1/2} \lambda^\star \in \mathbb{R}^{n_x}$. By composing (24) and (26), we obtain

$$V_\eta(\eta, t) \leq 0 \iff$$
$$\eta \in \left\{ Q_0^{\frac{1}{2}} v + \sum_{i=1}^{n_w} \int_0^t \bar{D}_i(\tau) \text{sgn}\left(v^\top Q_0^{-\frac{1}{2}} \bar{D}_i(\tau)\right) d\tau \middle| ||v||_2^2 \leq 1 \right\}.$$

As mentioned in (12), the FRS is the sub-zero level set of the value function. Therefore, the set in the above expression represents the FRS $\mathscr{E}_\eta(t)$. □

Note that $\mathscr{E}_\eta(t)$ can be interpreted as the Minkowski sum of sets as

$$\begin{aligned} &\mathscr{E}_\eta(t) = \mathscr{E}_0 \oplus \mathscr{D}(t), \quad \mathscr{D}(t) = \bigoplus_{i=1}^{n_w} \mathscr{D}_i(t), \\ &\mathscr{D}_i(t) = \left\{ \int_0^t \bar{D}_i(\tau) \text{sgn}\left(v^\top Q_0^{-\frac{1}{2}} \bar{D}_i(\tau)\right) d\tau \middle| ||v||_2^2 \leq 1 \right\}, \end{aligned} \tag{27}$$

where $\mathscr{D}_i$ is the reachable set due to the i-th channel of disturbance $w_i(t)$. Although we analyze how the FRS $\mathscr{E}_\eta(t)$ is composed of, how this can be computed is still obscure since numerical integration is required to compute $\mathscr{D}_i(t)$. Moreover, the numerical computation of the Minkowski sum of sets is intractable as the number of state increases. Methods for overcoming those limitations are discussed in the next section.

IV. Propagation of the Forward Reachable Set

This section discusses an efficient way to describe an approximation of the error FRS. We first figure out an ellipsoid which encloses $\mathscr{D}_i(t)$ of (27). Then, we compose ellipsoidal regions to find the resultant ellipsoid which encompasses the original FRS expressed in (12). Finally, the propagation law for the ellipsoidal FRSs is derived and used for the robust trajectory planning problem.

A. Ellipsoidal approximation on $\mathscr{D}_i(t)$

The following proposition presents the expression for the conservatively approximated region of $\mathscr{D}_i(t)$.

Proposition 2. Let $Q_i(t) \in \mathbb{S}^{n_x}_{++}$ be a shape matrix of an ellipsoid for $i \in [1, n_w]$. The set $\mathscr{D}_i(t)$ is encompassed by $Q_i(t)$ if

$$Q_i(t) = t \int_0^t \left(\bar{D}_i(\tau)\bar{D}_i(\tau)^\top + \varepsilon I\right) d\tau,$$

where ε is an arbitrary positive scalar, and I is the $n_x \times n_x$ identity matrix.

Proof. It suffices to show

$$d(t)^\top Q_i(t)^{-1} d(t) - 1 \leq 0, \quad \forall d(t) \in \mathscr{D}_i(t). \tag{28}$$

Substituting $Q_i(t)$ into (28) yields

$$t - d(t)^\top \left(\int_0^t \left(\bar{D}_i(\tau)\bar{D}_i(\tau)^\top + \varepsilon I \right) d\tau \right)^{-1} d(t) \geq 0. \quad (29)$$

Note that the left-hand side of (29) is the Schur complement of the following matrix

$$S(t) = \begin{bmatrix} t & d(t)^\top \\ d(t) & \int_0^t \left(\bar{D}_i(\tau)\bar{D}_i(\tau)^\top + \varepsilon I \right) d\tau \end{bmatrix}.$$

Let $m(\tau) = \text{sgn}(v^\top Q_0^{-\frac{1}{2}} \bar{D}_i(\tau))$, $\tau \in [0,t]$. We first consider the case when $m(\tau)$ is constant, and then the case when $m(\tau)$ varies over τ.

Case 1) Suppose that $m(\tau) = 1$, $\forall \tau \in [0,t]$. Then, $d(t) = \int_0^t \bar{D}_i(\tau) d\tau$. Now $S(t)$ can be expressed as

$$S(t) = \int_0^t s(\tau) d\tau, \quad s(\tau) = \begin{bmatrix} 1 & \bar{D}_i(\tau)^\top \\ \bar{D}_i(\tau) & \bar{D}_i(\tau)\bar{D}_i(\tau)^\top + \varepsilon I \end{bmatrix}.$$

Note that $s(\tau)$ and $S(t)$ are positive definite matrices, and the right bottom block of $S(t)$ is also positive definite. From the positive semi-definiteness condition, the Schur complement of $S(t)$ is determined as positive semi-definite, which validates the inequality of (29). When $m(\tau) = -1$, $\forall \tau \in [0,t]$, the same result can be derived similarly.

Case 2) Let $t' \in [0,t]$ be the moment when $m(\tau)$ changes. Assume that $m(\tau) = 1$ if $\tau < t'$ and $m(\tau) = -1$ if $\tau \geq t'$. In this case, $S(t)$ can be expressed as the sum of two matrices

$$S(t) = \int_0^{t'} a(\tau) d\tau + \int_{t'}^t b(\tau) d\tau,$$
$$a(\tau) = \begin{bmatrix} 1 & \bar{D}_i(\tau)^\top \\ \bar{D}_i(\tau) & \bar{D}_i(\tau)\bar{D}_i(\tau)^\top + \varepsilon I \end{bmatrix},$$
$$b(\tau) = \begin{bmatrix} 1 & -\bar{D}_i(\tau)^\top \\ -\bar{D}_i(\tau) & \bar{D}_i(\tau)\bar{D}_i(\tau)^\top + \varepsilon I \end{bmatrix}.$$

Since all matrices that compose $S(t)$ are positive definite, the Schur complement of $S(t)$, i.e. the left-hand side of (29), is positive semi-definite from the property of the Schur complement. □

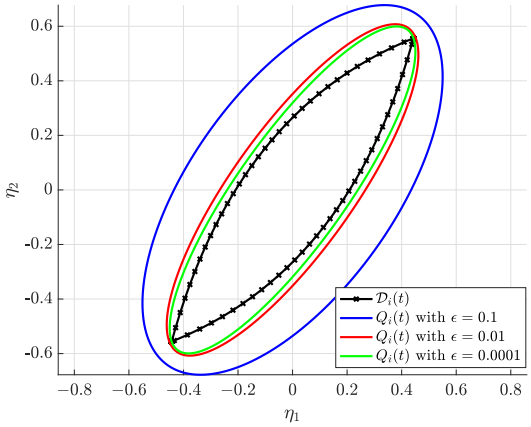

Fig. 2. Illustrative result of the approximation on $\mathcal{D}_(t)$ for a 2-state system: $\dot{e}_1 = e_2 + w_1 + 0.5w_2$, $\dot{e}_2 = -e_1 - e_2 + 0.4w_1 + w_2$ with $\bar{w} = [1.1\ 1.5]^\top$. The black dotted line represents the boundary of $\mathcal{D}_i(t)$. The blue, red, and green lines represent the approximation $Q_i(t)$ with $\varepsilon = 0.1$, $\varepsilon = 0.01$, and $\varepsilon = 0.0001$ respectively.

The computation of $Q_i(t)$ does not require any numerical integration. Considering that $\bar{D}_i(t) = \exp(-\Phi t) D_i(t) \bar{w}_i$, $Q_i(t)$ can be expressed as

$$Q_i(t) - \varepsilon t^2 I = \int_0^t \exp(-\Phi\tau) N_i(t) \exp(-\Phi^\top \tau) d\tau,$$
$$N_i(t) = t\bar{w}_i^2 D_i(t) D_i(t)^\top,$$

and thus $Q_i(t)$ is the solution of the following Lyapunov equation:

$$\begin{aligned} &-\Phi(Q_i(t) - \varepsilon t^2 I) - (Q_i(t) - \varepsilon t^2 I)\Phi^\top \\ &\quad = \exp(-\Phi t) N_i(t) \exp(-\Phi^\top t) - N_i(t). \end{aligned} \quad (30)$$

Note that the positive scalar ε can be selected sufficiently small in order to compute a less conservative approximation on $\mathcal{D}_i(t)$ as illustrated in Fig. 2.

B. Propagation of the ellipsoidal FRSs

This section provides an expression for the ellipsoid that encompasses the error FRS and how this ellipsoid varies according to time. Recall from (27) that the reachable set propagated by disturbances $\mathcal{D}(t)$ is the Minkowski sum of $\mathcal{D}_i(t)$. So, $\mathcal{D}(t)$ can be conservatively approximated by the Minkowski sum of $Q_i(t)$ as

$$\mathcal{D}_i(t) \subset \mathcal{B}(Q_i(t)) \Rightarrow \bigoplus_{i=1}^{n_w} \mathcal{D}_i(t) \subset \bigoplus_{i=1}^{n_w} \mathcal{B}(Q_i(t)),$$

where $\mathcal{B}(Q) \subset \mathbb{R}^{n_x}$ is the region occupied by an ellipsoid Q.

We utilize the formula for the ellipsoidal bounding of the Minkowski sum of ellipsoids [21] which represents

$$\begin{aligned} &\bigoplus_{i=1}^{n_w} \mathcal{B}(Q_i(t)) \subset \mathcal{B}(Q_d(t)) \\ &\iff Q_d(t) = \sum_{i=1}^{n_w} \frac{Q_i(t)}{r_i} \quad s.t. \sum_{i=1}^{n_w} r_i = 1. \end{aligned} \quad (31)$$

Since our interest is to get a conservative and compact approximation, r_i in (31) is selected so that the trace of Q_d(t) is as small as possible. A simple optimization on the trace of $Q_d(t)$ yields

$$Q_d(t) = \left(\sum_{i=1}^{n_w} \sqrt{tr(Q_i(t))} \right) \left(\sum_{i=1}^{n_w} \frac{Q_i(t)}{\sqrt{tr(Q_i(t))}} \right). \quad (32)$$

An ellipsoidal approximation on the reachable set in η-space, $\mathcal{E}_\eta(t)$ of (27), satisfies $\mathcal{E}_\eta(t) \subset \mathcal{B}(Q_0 \oplus Q_d(t))$. Considering the coordinate transform (13), the error state FRS $\mathcal{E}(t)$ is approximated with an ellipsoid $Q(t) \in \mathbb{S}^{n_x}_{++}$ as $\mathcal{E}(t) \subset \mathcal{B}(Q(t))$ where

$$Q(t) = \exp(\Phi t) \left(\left(1 + \frac{b}{a}\right) Q_0 + \left(1 + \frac{a}{b}\right) Q_d(t) \right) \exp(\Phi^\top t), \quad (33)$$

with $a = \sqrt{tr(Q_0)}$ and $b = \sqrt{tr(Q_d(t))}$. Until now we have derived the error FRS after a small duration t, starting from the initial ellipsoid Q_0. By using the computed $Q(t)$ as an initial ellipsoid at each t, the propagated ellipsoid after a small time dt, namely $Q(t+dt)$, can be consecutively derived using (30), (32), and (33).

Note that the proposed propagation law for the ellipsoidal error FRSs does not require any computationally burdensome procedure, such as a numerical optimization. This is because we have started from the analytic solution of the HJ PDE, and then sequentially approximate the solution sets as conservative ellipsoids. So, the ellipsoidal FRSs can be calculated quickly even though system parameters such as feedback gains $K(t)$ and disturbance bounds $\bar{w}$ vary over time. The real-time compatibility and capability to actively manage varying circumstances of the proposed method enable the safety-guaranteed trajectory planning discussed in the following section.

C. Robust trajectory planning with the ellipsoidal FRSs

Based on the findings from the previous sections, the original trajectory planning problem (6) is solved with existing numerical optimization techniques. Since the FRSs can be propagated independently of the trajectory planning procedure, any optimization algorithm which can handle nonlinear constraints can be employed. We make use of the constrained version of differential dynamic programming (DDP) [22] to satisfy collision avoidance constraints.

Rather than considering a single state $\underline{x}(t)$ in avoiding a collision, we set the distance between the FRS ellipsoid and an obstacle ellipsoid as the collision constraints. Let $\mathscr{B}(x_{obs}, Q_{obs})$ denote the region occupied by the obstacle, where $x_{obs} \in \mathbb{R}^{n_x}$ and $Q_{obs} \in \mathbb{S}^{n_x}_{++}$. For all states in $\mathscr{X}(t)$ to avoid collision with the obstacle, the Minkowski sum of the FRS ellipsoid and the obstacle ellipsoid $Q(t) \oplus Q_{obs}$ must not contain the difference between the nominal state and the obstacle state, $\underline{x}(t) - x_{obs}$. Thus, the robust collision avoidance constraint can be written as

$$c(\mathscr{X}(t)) = (\underline{x}(t) - x_{obs})^\top (Q(t) \oplus Q_{obs})^{-1} (\underline{x}(t) - x_{obs}) - 1. \tag{34}$$

Fig. 3 illustrates a simple robust planning simulation for the 2-state system. The nominal trajectory is generated so that the ellipsoidal FRSs do not intersect with the obstacle regions. To validate that the state trajectory is certainly bounded by the generated ellipsoidal FRSs, we randomly sample some states in the initial set and then propagate them with the control input (3) and the optimal disturbance (21). All of the sampled states remain inside of the ellipsoidal FRSs and arrive inside of $\mathscr{X}(2)$ at $t = 2$.

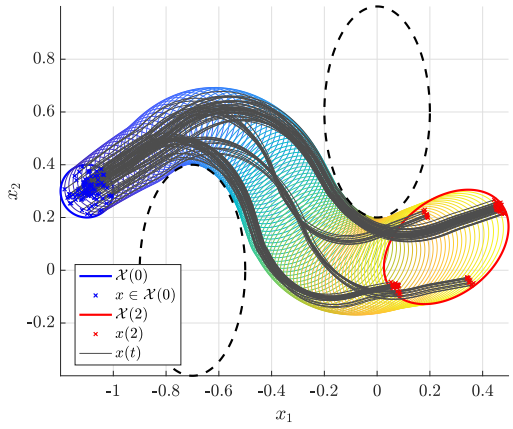

Fig. 3. Illustrative simulation for the 2-state system discussed in Fig. 2. The blue and red lines at each end represent boundaries of $\mathscr{X}(0)$ and $\mathscr{X}(2)$ respectively. The colored thin lines denote boundaries of $\mathscr{X}(t)$. The blue dots are randomly selected initial states which are contained in $\mathscr{X}(0)$. The black lines are state trajectories from each initial state, and the red dots represent end points of the trajectories. The black dashed lines denote obstacle regions.

V. Experimental Validation

A. Scenario

We conduct flight tests on avoiding obstacles in an environment with wind disturbance as illustrated in Fig. 1. The multirotor tries to follow the predefined reference trajectory which passes through the windy area. We compare the results of two experiments. In the first experiment, the size of the ellipsoidal FRSs is modified when the multirotor enters the windy region, according to the estimates on disturbances due to wind. In the second experiment, disturbance bounds are not estimated, so the ellipsoidal FRSs are propagated as if there exists no external disturbance.

B. Setups

We use a DJI F450 multirotor with E800 motors controlled by 620S electronic speed controllers. A Pixhawk autopilot [23] is attached at the center of the multirotor and connected to an onboard computer via USB. We use Intel NUC (8 GB memory with quad-core i7-7567U at 3.5 GHz) running Ubuntu 16.04 as the onboard computer. Measurements from VICON are sent to the onboard computer via Crazyradio 2.4 GHz radio telemetry. All of the control, trajectory planning, and the proposed FRS propagation algorithms are implemented on the onboard computer.

For online trajectory generation, we implement [22] in C++ and solve (6) with 200 prediction horizons and 0.02 seconds of time step, i.e. $dt = 0.02$ and $T = 4$. The cost function of (6) is composed of the distance to the reference trajectory and input regulation. The position and size of obstacles are assumed to be known. The robust collision avoidance constraints are implemented as in (34). The optimal $\underline{x}(t)$ and $\underline{u}(t)$ are sent to the control module and the resultant control input $u(t)$ is computed as (3) with the constant feedback gain

$$K(t) = \begin{bmatrix} 0 & 0 & -8 & 0 & 0 & -6 & 0 & 0 \\ 0 & 5 & 0 & 0 & 4 & 0 & -8 & 0 \\ -5 & 0 & 0 & -4 & 0 & 0 & 0 & -8 \end{bmatrix}.$$

The computed $u(t)$ is sent to the autopilot using MAVROS for the low-level control implemented in the Pixhawk.

We also implement the disturbance estimation algorithm proposed in [24]. The estimated values are used to modify the disturbance bounds of the proposed FRS propagation algorithm. We set the disturbance bound $\bar{w} = [0.5\ 0.5\ 0.5]^\top$ in the normal flight condition. Also, the increased bound $\bar{w} = [0.5\ 2.0\ 0.5]^\top$ is used when the multirotor is in wind of 4 m/s. The disturbance bound on the y-axis is only changed since external disturbances are dominant along the y-axis in our environment.

C. Results

Fig. 4 describes the states of the multirotor and the corresponding sets of states computed form the proposed algorithm. When the multirotor enters the windy region, the disturbance bound is changed according to the estimated value. As a result, the size of the reachable sets is adjusted as can be seen at 61 and 73 seconds of Fig. 4. The propagated FRSs certainly enclose the states of the multirotor, regardless of the external disturbances.

The first three columns of Fig. 5 illustrates how multirotor avoids obstacles. Considering the updated reachable sets, the nominal trajectory is modified in a safer direction when the multirotor is in a risky area. Therefore, safety-guaranteed flight trajectory is generated, resulting in successful obstacle avoidance in the disturbed environment. The result of the failed case is described in the last column of Fig. 5. The multirotor collides with the obstacle because the computed FRSs cannot guarantee that the state always stays in the FRSs when the multirotor is affected by wind, without modifying the disturbance bound. Table 1 validates a real-time robust trajectory planning is available.

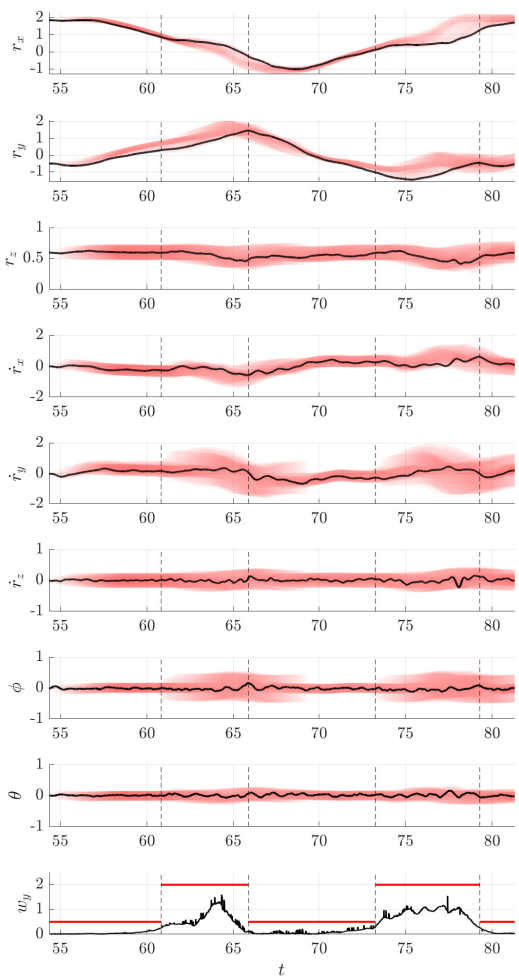

Fig. 4. State histories of the multirotor and the estimated disturbance. The black line represents the measured value, and the region shaded with red represents the FRSs over time. The red line is the disturbance bound on the y-axis.

VI. Conclusion

This paper presents a robust trajectory generation method based on the HJ reachability analysis. We first investigate the reachability problem with HJ PDE and compute the solution, i.e. the reachable sets of states, under the conditions of feedback control policy and system linearization. Started from the analytic solution of the reachable set, we parameterize the reachable set as an ellipsoid which encloses the boundary of the set. By using the ellipsoidal reachable set in trajectory optimization, we can generate the trajectory which robustly guarantees the safety of the system. The ellipsoidal parameterization enables a real-time computation of the reachable set, so safety-guaranteed planning is available even if the system encounters unexpected disturbances. The flight experiment of avoiding obstacles in the disturbed environment presents the validity and versatility of the proposed method.

References

[1] Charles Richter, Adam Bry, and Nicholas Roy. Polynomial trajectory planning for aggressive quadrotor flight in dense indoor environments. In *Robotics Research*, pages 649–666. Springer, 2016.

[2] Helen Oleynikova, Michael Burri, Zachary Taylor, Juan Nieto, Roland Siegwart, and Enric Galceran. Continuous-time trajectory optimization for online uav replanning. In *Intelligent Robots and Systems (IROS), 2016 IEEE/RSJ International Conference on*, pages 5332–5339. IEEE, 2016.

[3] Vladyslav Usenko, Lukas von Stumberg, Andrej Pangercic, and Daniel Cremers. Real-time trajectory replanning for mavs using uniform b-splines and a 3d circular buffer. In *Intelligent Robots and Systems (IROS), 2017 IEEE/RSJ International Conference on*, pages 215–222. IEEE, 2017.

[4] Jing Chen, Tianbo Liu, and Shaojie Shen. Online generation of collision-free trajectories for quadrotor flight in unknown cluttered environments. In *Robotics and Automation (ICRA), 2016 IEEE International Conference on*, pages 1476–1483. IEEE, 2016.

[5] Sikang Liu, Michael Watterson, Kartik Mohta, Ke Sun, Subhrajit Bhattacharya, Camillo J Taylor, and Vijay Kumar. Planning dynamically feasible trajectories for quadrotors using safe flight corridors in 3-d complex environments. *IEEE Robotics and Automation Letters*, 2(3):1688–1695, 2017.

[6] Jean-Marie Kai, Guillaume Allibert, Minh-Duc Hua, and Tarek Hamel. Nonlinear feedback control of quadrotors exploiting first-order drag effects. *IFAC-PapersOnLine*, 50(1):8189–8195, 2017.

[7] Ian M Mitchell, Alexandre M Bayen, and Claire J Tomlin. A time-dependent hamilton-jacobi formulation of reachable sets for continuous dynamic games. *IEEE Transactions on automatic control*, 50(7):947–957, 2005.

[8] Anirudha Majumdar and Russ Tedrake. Funnel libraries for real-time robust feedback motion planning. *The International Journal of Robotics Research*, 36(8):947–982, 2017.

[9] Suseong Kim, Davide Falanga, and Davide Scaramuzza. Computing the forward reachable set for a multirotor under first-order aerodynamic effects. *IEEE Robotics and Automation Letters*, 3(4):2934–2941, 2018.

[10] Sylvia L Herbert, Mo Chen, SooJean Han, Somil Bansal, Jaime F Fisac, and Claire J Tomlin. Fastrack: a modular framework for fast and guaranteed safe motion planning. In *Decision and Control (CDC), 2017 IEEE 56th Annual Conference on*, pages 1517–1522. IEEE, 2017.

Procedure		CPU time	%
DDP	Forward pass	13.7 ms	18.9 %
	Backward pass	56.3 ms	77.8 %
Propagation of ellipsoidal FRS		2.4 ms	3.3 %
Total		72.4 ms	100 %

TABLE I

Computation time of the proposed trajectory planning.

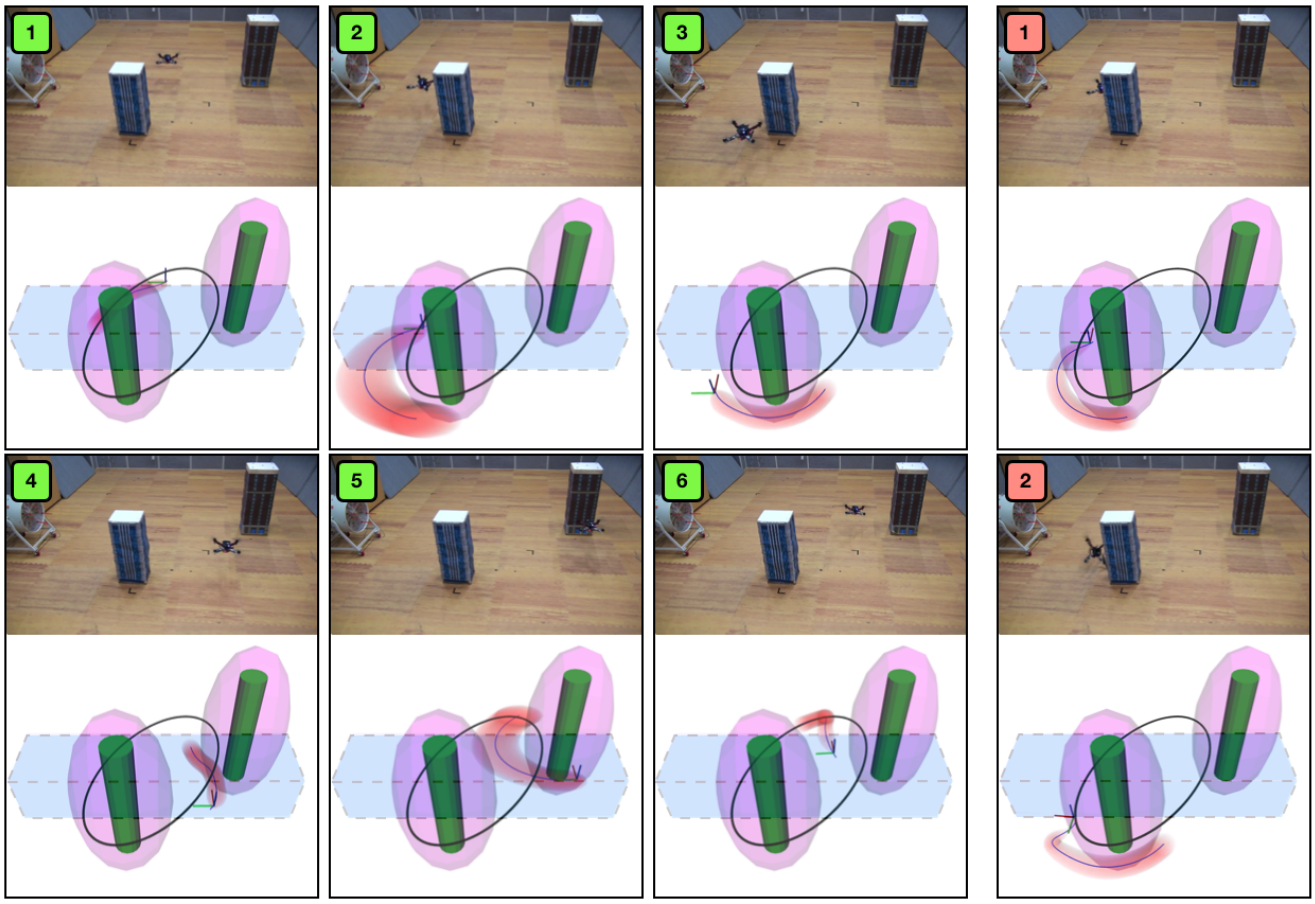

Fig. 5. Results of the robust trajectory planning in unknown wind disturbance. The shaded blue region is the area affected by wind, and the green cylinders and magenta ellipsoids are the actual and inflated shape of obstacles. The blue line represents the optimized nominal trajectory and the colored axes on the trajectory denote the current pose of the multirotor. The red ellipsoids surrounding the nominal trajectory are the FRSs of the multirotor. The thick black solid line denotes the predefined reference trajectory. The first three columns (numbered 1–6 in green) represent the success case, where each snapshot is taken at 58, 62, 66, 73, 77, and 80 seconds respectively. The last column (1 and 2 in red) represents the failed case.

[11] David Fridovich-Keil, Sylvia L Herbert, Jaime F Fisac, Sampada Deglurkar, and Claire J Tomlin. Planning, fast and slow: A framework for adaptive real-time safe trajectory planning. *arXiv preprint arXiv:1710.04731*, 2017.

[12] Mario E Villanueva, Boris Houska, and Benoît Chachuat. Unified framework for the propagation of continuous-time enclosures for parametric nonlinear odes. *Journal of Global Optimization*, 62(3):575–613, 2015.

[13] Mario E Villanueva, Rien Quirynen, Moritz Diehl, Benoît Chachuat, and Boris Houska. Robust mpc via min–max differential inequalities. *Automatica*, 77:311–321, 2017.

[14] Somil Bansal, Mo Chen, Sylvia Herbert, and Claire J Tomlin. Hamilton-jacobi reachability: A brief overview and recent advances. In *Decision and Control (CDC), 2017 IEEE 56th Annual Conference on*, pages 2242–2253. IEEE, 2017.

[15] Daniel Mellinger, Nathan Michael, and Vijay Kumar. Trajectory generation and control for precise aggressive maneuvers with quadrotors. *The International Journal of Robotics Research*, 31(5):664–674, 2012.

[16] Matthias Faessler, Antonio Franchi, and Davide Scaramuzza. Differential flatness of quadrotor dynamics subject to rotor drag for accurate tracking of high-speed trajectories. *IEEE Robot. Autom. Lett*, 3(2):620–626, 2018.

[17] Jérôme Darbon and Stanley Osher. Algorithms for overcoming the curse of dimensionality for certain hamilton–jacobi equations arising in control theory and elsewhere. *Research in the Mathematical Sciences*, 3(1):19, 2016.

[18] Matthew R Kirchner, Robert Mar, Gary Hewer, Jérôme Darbon, Stanley Osher, and Yat Tin Chow. Time-optimal collaborative guidance using the generalized hopf formula. *IEEE Control Systems Letters*, 2(2):201–206, 2018.

[19] P-L Lions and J-C Rochet. Hopf formula and multitime hamilton-jacobi equations. *Proceedings of the American Mathematical Society*, 96(1):79–84, 1986.

[20] Jérôme Darbon. On convex finite-dimensional variational methods in imaging sciences and hamilton–jacobi equations. *SIAM Journal on Imaging Sciences*, 8(4):2268–2293, 2015.

[21] AB Kurzhanski and TF Filippova. On the theory of trajectory tubes—a mathematical formalism for uncertain dynamics, viability and control. In *Advances in nonlinear dynamics and control: a report from Russia*, pages 122–188. Springer, 1993.

[22] Brian Plancher, Zachary Manchester, and Scott Kuindersma. Constrained unscented dynamic programming. In *2017 IEEE/RSJ International Conference on Intelligent Robots and Systems (IROS)*, pages 5674–5680. IEEE, 2017.

[23] Lorenz Meier, Petri Tanskanen, Friedrich Fraundorfer, and Marc Pollefeys. Pixhawk: A system for autonomous flight using onboard computer vision. In *2011 IEEE International Conference on Robotics and Automation*, pages 2992–2997. IEEE, 2011.

[24] Suseong Kim, Seungwon Choi, Hyeonggeun Kim, Jongho Shin, Hyungbo Shim, and H Jin Kim. Robust control of an equipment-added multirotor using disturbance observer. *IEEE Transactions on Control Systems Technology*, 26(4):1524–1531, 2018.